

Production of heavy neutron-rich nuclei with radioactive beams in multinucleon transfer reactions

Cheng Li^{1,2} · Peiwei Wen^{1,2} · Jingjing Li^{1,2} · Gen Zhang^{1,2} · Bing Li^{1,2} · Feng-Shou Zhang^{1,2,3}

Received: 12 January 2017/Revised: 12 April 2017/Accepted: 16 April 2017/Published online: 29 June 2017

© Shanghai Institute of Applied Physics, Chinese Academy of Sciences, Chinese Nuclear Society, Science Press China and Springer Nature Singapore Pte Ltd. 2017

Abstract The production mechanism of heavy neutron-rich nuclei is investigated by using the multinucleon transfer reactions of $^{136,148}\text{Xe}+^{208}\text{Pb}$ and $^{238}\text{U}+^{208}\text{Pb}$ in the framework of a dinuclear system model. The evaporation residual cross sections of target-like fragments are studied with the reaction system $^{148}\text{Xe}+^{208}\text{Pb}$ at near barrier energies. The results show that the final isotopic production cross sections in the neutron-deficient side are very sensitive to incident energy while it is not sensitive in the neutron-rich side. Comparing the isotopic production cross sections for the reactions of ^{208}Pb bombarded with stable and radioactive projectiles, we find that neutron-rich radioactive beams can significantly increase the production cross sections of heavy neutron-rich nuclei.

Keywords Multinucleon transfer reactions · DNS model · Heavy-ion collisions · Neutron-rich nuclei

1 Introduction

Production of new heavy neutron-rich nuclei has attracted widespread interests in recent years [1–11]. The production of these exotic nuclei located far from the stability line is very important for exploring their structure and decay properties [12, 13], as well as a measurement of spins, neutron skin thickness [14], magnetic dipole, and electric quadrupole moments and charge radii, *et al.* In addition, it is also extremely important for understanding the r-process in nuclear astrophysics. The r-process path is located (and interrupted by fission) just in the region of unknown heavy nuclei with a large neutron excess. The neutron closed shell $N = 126$ is probably the last “waiting point” in the r-process of nucleosynthesis [15]. It is helpful for answering the origin of heavy elements from iron to uranium in the Universe.

Many new neutron-rich nuclei are produced by experiment with fragmentation method of projectile [16, 17]. For example, there are 60 new neutron-rich isotopes in the atomic number range of $60 \leq Z \leq 78$ produced by using a 1 GeV/nucleon ^{238}U beam impinged on a ^9Be target by Kurcewicz *et al.* at GSI Darmstadt [16]. They found that the fragmentation plays a dominant role in the production of the isotopes of the elements above $Z = 72$. However, production cross sections of these nuclei with the fragmentation method are very small and are about a few ten pb orders of magnitude. It is difficult for further production of more neutron-rich nuclei with the fragmentation method. Recently, a multinucleon transfer (MNT) reaction experiment of $^{136}\text{Xe}+^{198}\text{Pt}$ was performed by Watanabe *et al.* at GANIL in Caen [9]. They found that the MNT approach has

This work was supported by the National Natural Science Foundation of China under Grants Nos. 11635003, 11025524 and 11161130520; the National Basic Research Program of China under Grant No. 2010CB832903; the European Commission’s 7th Framework Programme (Fp7-PEOPLE-2010-IRSES) under Grant Agreement Project No. 269131; the Project funded by China Postdoctoral Science Foundation (Grant No. 2016M600956).

✉ Feng-Shou Zhang
fszhang@bnu.edu.cn

Cheng Li
licheng@mail.bnu.edu.cn

¹ The Key Laboratory of Beam Technology and Material Modification of Ministry of Education, College of Nuclear Science and Technology, Beijing Normal University, Beijing 100875, China

² Beijing Radiation Center, Beijing 100875, China

³ Center of Theoretical Nuclear Physics, National Laboratory of Heavy Ion Accelerator of Lanzhou, Lanzhou 730000, China

huge advantages for the production of very neutron-rich nuclei with $Z \leq 77$ compared to the above fragmentation approach. It demonstrates that the MNT route is a more promising path to produce new neutron-rich isotopes around $N = 126$ shell.

Radioactive ion beam facilities can provide very neutron-rich projectiles [18, 19] which could significantly improve the production cross section of heavy neutron-rich nuclei [20, 21]. Some facilities, such as the high-intensity heavy-ion accelerator facility (HIAF) in China [22, 23], have a plan to produce new heavy neutron-rich nuclei with intense secondary beams of exotic radioactive nuclei by the MNT reactions. Theoretical support for these very time-consuming and expensive experiments is vital for choosing the optimum target-projectile-energy combinations and for the estimation of cross sections. The dinuclear system (DNS) model is a semiclassical model which has shown reasonable success in predicting the evaporation residual cross section in fusion reactions [24–26] and multinucleon transfer reactions [27, 28]. In this work, we apply the DNS model to study the multinucleon transfer process with stable projectiles ^{136}Xe , ^{238}U , and radioactive projectile ^{148}Xe impinging on a ^{208}Pb target.

The structure of this paper is as follows. In Sect. 2, we briefly introduce the DNS model. In Sect. 3, the isotope production cross sections of $^{136}\text{Xe}+^{208}\text{Pb}$, $^{238}\text{U}+^{208}\text{Pb}$, and $^{148}\text{Xe}+^{208}\text{Pb}$ systems have been studied by using the DNS model. Finally, the conclusion is given in Sect. 4.

2 Theoretical descriptions

In the framework of the DNS model, the distribution probability can be obtained by solving a set of master equations numerically in the potential energy surface of the DNS. The probability distribution function $P(Z_1, N_1, E_1, t)$ for fragment 1 with proton number Z_1 , neutron number N_1 , and excitation energy E_1 is described by the following master equation [27, 29]:

$$\begin{aligned} & \frac{dP(Z_1, N_1, E_1, t)}{dt} \\ &= \sum_{Z'_1} W_{Z_1, N_1; Z'_1, N'_1}(t) [d_{Z_1, N_1} P(Z'_1, N_1, E'_1, t) \\ & \quad - d_{Z'_1, N'_1} P(Z_1, N_1, E_1, t)] \\ & \quad + \sum_{N'_1} W_{Z_1, N_1; Z_1, N'_1}(t) [d_{Z_1, N_1} P(Z_1, N'_1, E'_1, t) \\ & \quad - d_{Z_1, N'_1} P(Z_1, N_1, E_1, t)] \\ & \quad - [\Lambda_{Z_1, N_1}^{\text{qf}}(\Theta(t)) + \Lambda_{Z_1, N_1}^{\text{fis}}(\Theta(t))] P(Z_1, N_1, E_1, t). \end{aligned} \tag{1}$$

The sum is taken over all possible proton and neutron numbers that fragments Z'_1 and N'_1 may take, but only one

nucleon transfer is considered in the model with the relation $Z'_1 = Z_1 \pm 1$ and $N'_1 = N_1 \pm 1$. $W_{Z_1, N_1; Z'_1, N'_1}$ denotes the mean transition probability from channel (Z_1, N_1, E_1) to (Z'_1, N_1, E'_1) , which can be read as

$$\begin{aligned} W_{Z_1, N_1; Z'_1, N'_1} &= \frac{\tau_{\text{mem}}(Z_1, N_1, E_1; Z'_1, N_1, E'_1)}{\hbar^2 d_{Z_1, N_1} d_{Z'_1, N'_1}} \\ & \quad \times \sum_{ii'} |\langle Z'_1, N_1, E'_1, i' | V | Z_1, N_1, E_1, i \rangle|^2, \end{aligned} \tag{2}$$

where τ_{mem} and V denote memory time and single-particle potential, respectively. i denotes all remaining quantum numbers [30]. d_{Z_1, N_1} denotes the microscopic dimension corresponding to the macroscopic state (Z_1, N_1, E_1)

$$d(m_1, m_2) = \binom{n_1}{m_1} \binom{n_2}{m_2}. \tag{3}$$

The $n_1 = g_1 \Delta \varepsilon$ and $n_2 = g_2 \Delta \varepsilon$ denote the numbers of valence states of fragments 1 and 2, respectively. g_1 and g_2 are mean single-particle level densities. $\Delta \varepsilon = \sqrt{4\varepsilon^*/g}$ is an energy range around Fermi energy, ε_F , of both fragments. $m_1 = n_1/2$ and $m_2 = n_2/2$ denote corresponding numbers of valence nucleons [30, 31]. The quasifission rate $\Lambda_{Z_1, N_1}^{\text{qf}}$ and the fission rate $\Lambda_{Z_1, N_1}^{\text{fis}}$ of the heavy fragment are estimated with the one-dimensional Kramers formula [32]. $\Theta(t) = \sqrt{\varepsilon^*/a}$ is the local temperature. $a = A_i/12$ is the level-density parameter. We assume that ε^* is divided between the two primary fragments according to their mass ratio. Hence, the excitation energy of fragment 1 is expressed as $E_1 = A_1/(A_1 + A_2)\varepsilon^*$. A_1 and A_2 are mass numbers of fragment 1 and fragment 2, respectively.

The local excitation energy, ε^* , is defined as

$$\varepsilon^* = E^{\text{diss}} - [U(A_1, A_2) - U(A_P, A_T)]. \tag{4}$$

Here E^{diss} is the energy dissipation from the relative kinetic energy loss, which can be seen in Ref. [33]. The dissipation of the relative motion and angular momentum of the DNS is described by the Fokker–Planck equation. The $U(A_1, A_2)$ and $U(A_P, A_T)$ are the driving potentials at the configuration of (A_1, A_2) and at the entrance point of DNS, which can be read as

$$\begin{aligned} U(A_1, A_2, J, \mathbf{R}; \beta_1, \beta_2, \theta_1, \theta_2) &= B(Z_1, N_1) + B(Z_2, N_2) \\ & \quad - [B(Z, N) + V_{\text{rot}}^{\text{CN}}(J)] \\ & \quad + V(A_1, A_2, J, \mathbf{R}; \beta_1, \beta_2, \theta_1, \theta_2). \end{aligned} \tag{5}$$

where $B(Z_1, N_1)$, $B(Z_2, N_2)$, and $B(Z, N)$ are the binding energies of the fragment 1, fragment 2, and the compound nucleus, respectively, in which the shell and the pairing corrections are included reasonably. $V_{\text{rot}}^{\text{CN}}$ is the rotation

energy of the compound nucleus. The β_1 and β_2 are quadrupole deformation parameters of the two fragments at ground state which is static in the nucleon transfer process. θ_1 and θ_2 are angles between the collision orientations and the symmetry axes for fragment 1 and fragment 2, respectively. In Ref. [27], the calculations show that the tip–tip and side–side collisions give a similar result in the isotope distributions of $^{238}\text{U}+^{238}\text{U}$ collisions at incident energy near $1.1 V_C$. Hence, in this work, only tip–tip cases are considered for calculations. The interaction potential between two fragments includes nuclear, Coulomb, and centrifugal parts

$$\begin{aligned}
 V(A_1, A_2, J, \mathbf{R}; \beta_1, \beta_2, \theta_1, \theta_2) \\
 = V_N(A_1, A_2, \mathbf{R}; \beta_1, \beta_2, \theta_1, \theta_2) \\
 + V_C(A_1, A_2, \mathbf{R}; \beta_1, \beta_2, \theta_1, \theta_2) + \frac{J(J+1)\hbar^2}{2\mu\mathbf{R}^2},
 \end{aligned}
 \tag{6}$$

where μ is the reduced mass of system. The nuclear potential is calculated by using the double-folding method. The Coulomb potential is obtained by Wong’s formula [31].

The cross sections of the primary fragments (Z_1, N_1) are calculated as follows

$$\begin{aligned}
 \sigma_{\text{pr}}(Z_1, N_1, E_{\text{c.m.}}) \approx \frac{\pi\hbar^2}{2\mu E_{\text{c.m.}}} \sum_{J=0}^{J_{\text{max}}} (2J+1) T(E_{\text{c.m.}}, J) \\
 \times [P(Z_1, N_1, \tau_{\text{int}}) + Y_{Z_1, N_1}],
 \end{aligned}
 \tag{7}$$

where $T(E_{\text{c.m.}}, J)$ is the capture probability. $P(Z_1, N_1, \tau_{\text{int}})$ is the formation probability of primary fragments from the equilibrium state of DNS. The contribution of fission rate is ignored in this work. The Y_{Z_1, N_1} denotes the primary yields of fragments from the quasifission rate [32, 34], which is written as

$$Y_{Z_1, N_1} = \int_0^{\tau_{\text{int}}} \Lambda_{Z_1, N_1}^{\text{qf}} P(Z_1, N_1, E_1, t) dt.
 \tag{8}$$

The interaction time, τ_{int} , in the dissipation process of two colliding partners is dependent on the incident energy, $E_{\text{c.m.}}$, in the center-of-mass frame and the angular momentum, J , which is calculated by using the deflection function method and has the value of a few 10^{-20} s. For heavy systems with no potential pocket, the distance, \mathbf{R} , between the centers of the two fragments is chosen to be the value at the touching point, in which the DNS is assumed to be formed. The maximal angular momentum is taken as the grazing collisions. More detailed descriptions of the DNS model can be found in Refs. [30, 31].

To obtain the final isotope cross section distributions, we apply the GEMINI to deal with the subsequent de-excitation process of primary fragments. The GEMINI is a Monte

Carlo code which follows the decay of a compound nuclei by a series of sequential binary decays until the resulting products are unable to undergo any further decay. It allows not only light-particle emission and symmetric fission, but also the decaying nucleus to emit a fragment of any mass [35]. Nuclear level densities are taken as a Fermi-gas form with default parameters. In this work, we simulate 1000 times the de-excitation processes for each primary fragment.

To test the DNS model for the description of multinucleon transfer reactions, the isotopic production cross sections for $^{136}\text{Xe}+^{208}\text{Pb}$ at $E_{\text{c.m.}} = 450$ MeV are calculated by using the DNS model. Figure 1 shows the isotopic production cross sections from $Z = 78$ to 81. The dashed and solid lines denote the calculation results for primary and final fragments, respectively. The experimental data (solid circles) are from Ref. [2]. From Fig. 1, one can see that final yields shift to the left after the de-excitation process. The final isotopic cross sections are in good agreement with the experimental data. This indicates that the DNS model is applicable for the study of MNT reactions at near barrier energies.

3 Results and discussion

The radioactive neutron-rich nuclei have larger N/Z ratios. Such as ^{148}Xe is a known isotope of xenon with the largest neutron excess ($N/Z = 1.74$). It can be as a radioactive beam in the future. First, we discuss the isotopic cross sections in different incident energies. Figure 2 shows the primary isotopic cross sections of Pt at incident energies $E_{\text{c.m.}} = 1.02, 1.06,$ and $1.10 V_C$ for an

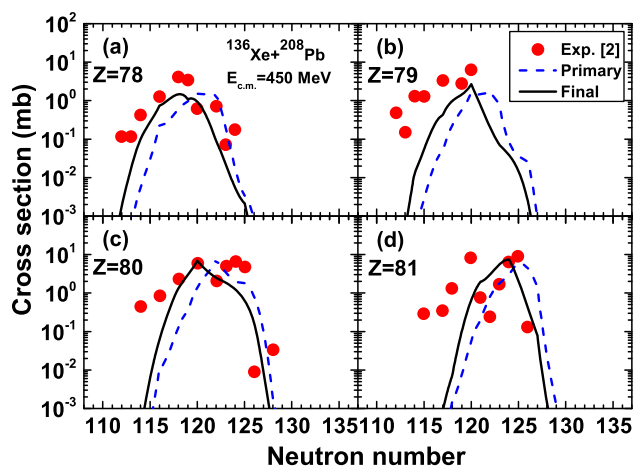


Fig. 1 (Color online) The isotopic production cross sections from $Z = 78$ to 81 for $^{136}\text{Xe}+^{208}\text{Pb}$ at $E_{\text{c.m.}} = 450$ MeV. The dashed and solid lines denote the calculation results for primary and final fragments, respectively. The experimental data (solid circles) are from Ref. [2]

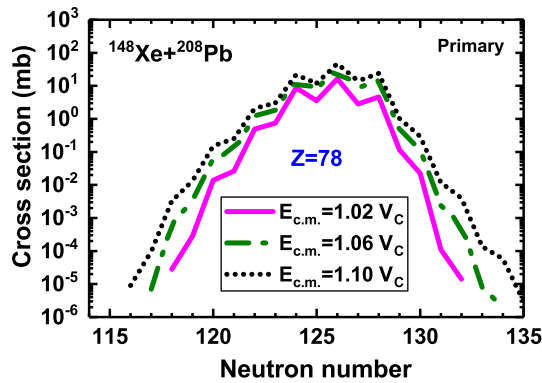


Fig. 2 (Color online) The primary isotopic cross section distributions of Pt at incident energy $E_{c.m.} = 1.02, 1.06$ and $1.10 V_C$ for $^{148}\text{Xe} + ^{208}\text{Pb}$ system. V_C is the Coulomb barrier

$^{148}\text{Xe} + ^{208}\text{Pb}$ system. V_C is the Coulomb barrier. The solid, dash-dotted and dotted lines denote the calculation results from incident energy $E_{c.m.} = 1.02, 1.06$, and $1.10 V_C$, respectively. One can see that isotopic cross sections increase with the increase in incident energies both in neutron-rich and neutron-deficient sides. Larger incident energy improves the transfer probability of nucleons on the same potential energy surface. However, larger incident energy will result in higher excitation energy for primary fragments.

Figure 3 shows the final isotopic production cross sections from $Z = 75$ to 80 for the reaction of $^{148}\text{Xe} + ^{208}\text{Pb}$ at different incident energies. One can see that in the neutron-deficient side, the isotopic production cross sections increase with increasing incident energies. It is very sensitive to incident energies. There are two reasons for this. One is that isotopic production cross sections in the neutron-deficient side at a larger incident energy are larger for primary fragments. The other one is that a larger incident energy leads to primary fragments obtaining more excitation energy. More neutrons evaporating causes a shift of final yields to the neutron-deficient side. While in the neutron-rich side, the final isotopic production cross sections are not sensitive to incident energies, especially for extremely neutron-rich nuclei. In addition, the values of peak for a few proton stripping channels change very slowly. Because of this, the driving potential of the system is reduced in the configuration of mass symmetry. The transfer of nucleons from target to projectile is dominant near the entrance point of DNS.

The N/Z ratio equilibration plays an important role between the projectile and target during the collision, which is one of the most important mechanisms to produce neutron-rich nuclei [36]. In Fig. 4, one shows the $N = 126$ isotones distributions for the reactions of $^{136}\text{Xe} + ^{208}\text{Pb}$ and $^{148}\text{Xe} + ^{208}\text{Pb}$ at different incident energies. From Fig. 4a, one can see that the cross sections of proton stripping

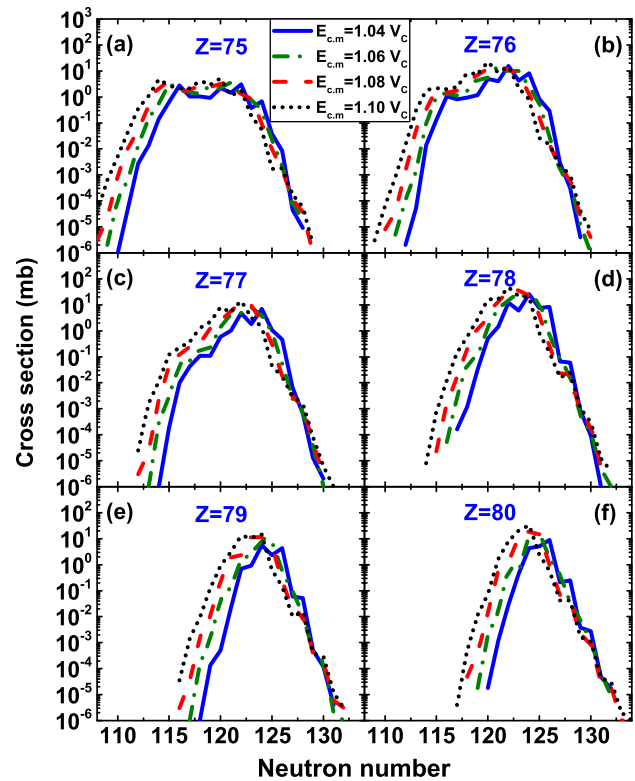


Fig. 3 (Color online) The final isotopic production cross section distributions from $Z = 75$ to 80 for the reaction of $^{148}\text{Xe} + ^{208}\text{Pb}$ at different incident energies

channels are slightly lower than the pickup channels. The nucleus produced in the $^{208}\text{Pb} + ^{136}\text{Xe}$ reaction with the largest neutron excess is only ^{204}Pt . It is because the N/Z value of ^{208}Pb (1.54) is larger than that of ^{136}Xe (1.52). It is hard to transfer protons from ^{208}Pb to ^{136}Xe , while in Fig. 4b, this phenomenon is opposite. The cross sections of proton stripping channels are obviously larger than the pickup channels. This reaction system can produce very neutron-rich nuclei (such as ^{199}Ta). Because the N/Z value of ^{148}Xe (1.74) is significantly larger than that of ^{208}Pb (1.54), the ^{208}Pb is easier to transfer protons to ^{148}Xe .

In Fig. 5, we show the isotope production cross sections of the ^{208}Pb target bombarded with stable projectiles ^{136}Xe , ^{238}U , and radioactive projectile, ^{148}Xe . The dashed, solid, and dotted lines denote the calculation results from $^{136}\text{Xe} + ^{208}\text{Pb}$, $^{238}\text{U} + ^{208}\text{Pb}$, and $^{148}\text{Xe} + ^{208}\text{Pb}$ systems at incident energy $E_{c.m.} = 1.10 V_C$. The open circles denote unknown neutron-rich nuclei. The N/Z values of ^{136}Xe , ^{238}U , and ^{148}Xe are 1.52, 1.59, and 1.74, respectively. One can see that the isotope production cross sections in the neutron-rich side for each panel increase with the increasing N/Z value of projectile. Especially for larger proton stripping channels, this trend is more significant. In Fig. 5a, b, there are 5 (for $Z = 75$) and 3 (for $Z = 76$)

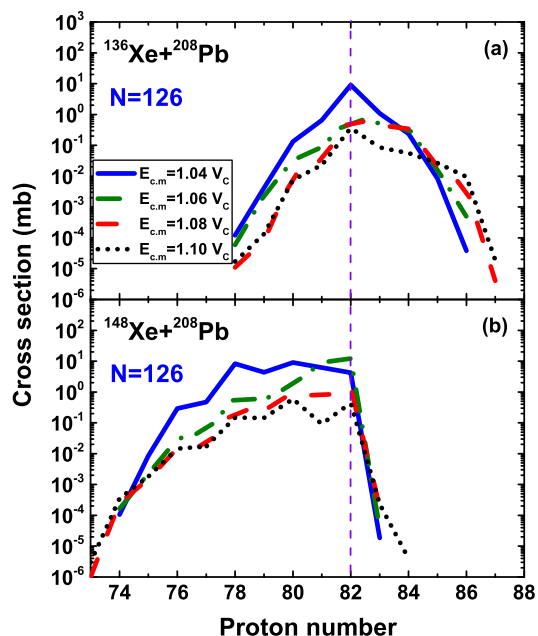


Fig. 4 (Color online) The $N = 126$ isotones distributions (final fragments) for the reactions of $^{136}\text{Xe}+^{208}\text{Pb}$ (up panel) and $^{148}\text{Xe}+^{208}\text{Pb}$ (bottom panel) at different incident energies

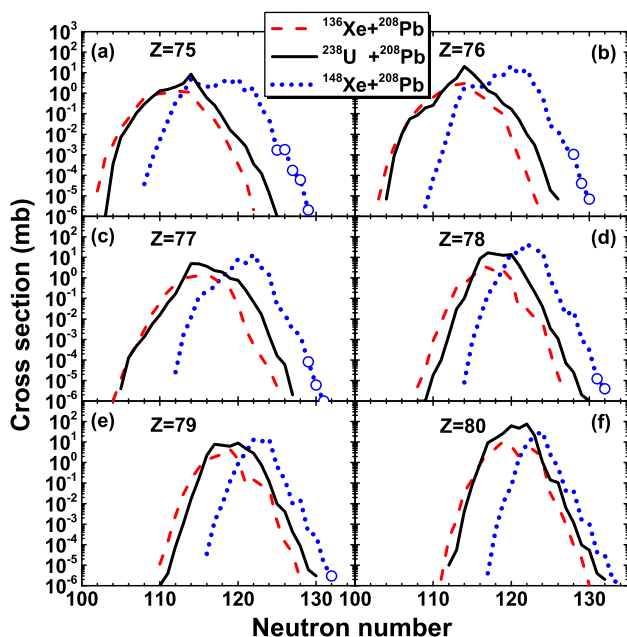


Fig. 5 (Color online) Final isotopic production cross sections with charge numbers from $Z = 75$ to 80 . The dashed, solid and dotted lines denote the calculation results from $^{136}\text{Xe}+^{208}\text{Pb}$, $^{238}\text{U}+^{208}\text{Pb}$ and $^{148}\text{Xe}+^{208}\text{Pb}$ systems at incident energy $E_{c.m.} = 1.10 V_c$. The open circles denote unknown neutron-rich nuclei

unknown neutron-rich nuclei produced by the $^{148}\text{Xe}+^{208}\text{Pb}$ reaction. This is because the exchange of particles between the two colliding partners is primarily driven by the N/Z

ratio equilibration. The very neutron-rich nuclei are easily produced by the reaction of $^{148}\text{Xe}+^{208}\text{Pb}$ via neutrons transfer. It can be seen that the production cross sections for the new neutron-rich nuclei $^{200-204}\text{Re}$ are 1.710, 1.810, 0.173, 0.060, and 0.002 μb , $^{204-206}\text{Os}$ are 1.040, 0.041, and 0.007 μb , $^{206-208}\text{Ir}$ are 0.081, 0.006, and 0.001 μb , $^{209,210}\text{Pt}$ are 0.012 and 0.004 μb , and ^{211}Au is 0.003 μb , respectively. Based on the above, the MNT reaction with the neutron-rich radioactive beams is a very effective method to produce new heavy neutron-rich nuclei.

4 Conclusion

In conclusion, the multinucleon transfer reactions of $^{136}\text{Xe}+^{208}\text{Pb}$, $^{238}\text{U}+^{208}\text{Pb}$, and $^{148}\text{Xe}+^{208}\text{Pb}$ are investigated using the DNS model. The isotopic production cross section of reaction $^{148}\text{Xe}+^{208}\text{Pb}$ at near barrier incident energies is studied. We find that the final isotopic production cross section of reaction $^{148}\text{Xe}+^{208}\text{Pb}$ in the neutron-deficient side is very sensitive to incident energies. For the neutron-rich nuclei, it is not sensitive to incident energies. The N/Z ratio equilibration plays an important role between the projectile and target during the collision. The cross sections of proton stripping channels are obviously larger than the pickup channels for the reaction of $^{148}\text{Xe}+^{208}\text{Pb}$ on $N = 126$ shell closure. The extremely neutron-rich projectile, ^{148}Xe , improves significantly the production cross sections of neutron-rich nuclei.

References

1. C. Li, F. Zhang, J.J. Li et al., Multinucleon transfer in the $^{136}\text{Xe}+^{208}\text{Pb}$ reaction. *Phys. Rev. C* **93**, 014618 (2016). doi:10.1103/PhysRevC.93.014618
2. J.S. Barrett, W. Loveland, R. Yanez et al., $^{136}\text{Xe}+^{208}\text{Pb}$ reaction: A test of models of multinucleon transfer reactions. *Phys. Rev. C* **91**, 064615 (2015). doi:10.1103/PhysRevC.91.064615
3. V.I. Zagrebaev, W. Greiner, Production of new heavy isotopes in low-energy multinucleon transfer reactions. *Phys. Rev. Lett.* **101**, 122701 (2008). doi:10.1103/PhysRevLett.101.122701
4. W. Loveland, A.M. Vinodkumar, D. Peterson et al., Synthesis of heavy nuclei using damped collisions: a test. *Phys. Rev. C* **83**, 044610 (2011). doi:10.1103/PhysRevC.83.044610
5. V.I. Zagrebaev, W. Greiner, Production of heavy trans-target nuclei in multinucleon transfer reactions. *Phys. Rev. C* **87**, 034608 (2013). doi:10.1103/PhysRevC.87.034608
6. V.I. Zagrebaev, W. Greiner, Production of heavy and superheavy neutron-rich nuclei in transfer reactions. *Phys. Rev. C* **83**, 044618 (2011). doi:10.1103/PhysRevC.83.044618
7. L. Zhu, J. Su, F.S. Zhang, Influence of the neutron numbers of projectile and target on the evaporation residue cross sections in hot fusion reactions. *Phys. Rev. C* **93**, 064610 (2016). doi:10.1103/PhysRevC.93.064610

8. K. Zhao, Z.X. Li, N. Wang et al., Production mechanism of neutron-rich transuranium nuclei in $^{238}\text{U} + ^{238}\text{U}$ collisions at near-barrier energies. *Phys. Rev. C* **92**, 024613 (2015). doi:[10.1103/PhysRevC.92.024613](https://doi.org/10.1103/PhysRevC.92.024613)
9. Y.X. Watanabe, Y.H. Kim, S.C. Jeong et al., Pathway for the production of neutron-rich isotopes around the $N = 126$ shell closure. *Phys. Rev. Lett.* **115**, 172503 (2015). doi:[10.1103/PhysRevLett.115.172503](https://doi.org/10.1103/PhysRevLett.115.172503)
10. K. Sekizawa, K. Yabana, Time-dependent Hartree–Fock calculations for multinucleon transfer processes in $^{40,48}\text{Ca} + ^{124}\text{Sn}$, $^{40}\text{Ca} + ^{208}\text{Pb}$, and $^{58}\text{Ni} + ^{208}\text{Pb}$ reactions. *Phys. Rev. C* **88**, 014614 (2013). doi:[10.1103/PhysRevC.88.014614](https://doi.org/10.1103/PhysRevC.88.014614)
11. K. Sekizawa, K. Yabana, Time-dependent Hartree–Fock calculations for multinucleon transfer and quasifission processes in the $^{64}\text{Ni} + ^{238}\text{U}$ reaction. *Phys. Rev. C* **93**, 054616 (2016). doi:[10.1103/PhysRevC.93.054616](https://doi.org/10.1103/PhysRevC.93.054616)
12. C.C. Guo, J. Su, F.S. Zhang, Comparison between nuclear thermometers in central $\text{Xe} + \text{Sn}$ collision. *Nucl. Sci. Tech.* **24**, 050513 (2013). doi:[10.13538/j.1001-8042/nst.2013.05.013](https://doi.org/10.13538/j.1001-8042/nst.2013.05.013)
13. C.W. Ma, C.Y. Qiao, T.T. Ding et al., Temperature of intermediate mass fragments in simulated $^{40}\text{Ca} + ^{40}\text{Ca}$ reactions around the Fermi energies by AMD model. *Nucl. Sci. Tech.* **27**, 111 (2016). doi:[10.1007/s41365-016-0112-8](https://doi.org/10.1007/s41365-016-0112-8)
14. X.F. Li, D.Q. Fang, Y.G. Ma, Determination of the neutron skin thickness from interaction cross section and charge-changing cross section for B, C, N, O, F isotopes. *Nucl. Sci. Tech.* **27**, 71 (2016). doi:[10.1007/s41365-016-0064-z](https://doi.org/10.1007/s41365-016-0064-z)
15. R. Wang, L.W. Chen, Positioning the neutron drip line and the r-process paths in the nuclear landscape. *Phys. Rev. C* **92**, 031303(R) (2015). doi:[10.1103/PhysRevC.92.031303](https://doi.org/10.1103/PhysRevC.92.031303)
16. J. Kurcewicz, F. Farinon, H. Geissel et al., Discovery and cross-section measurement of neutron-rich isotopes in the element range from neodymium to platinum with the FRS. *Phys. Lett. B* **717**, 371 (2012). doi:[10.1016/j.physletb.2012.09.021](https://doi.org/10.1016/j.physletb.2012.09.021)
17. O.B. Tarasov, D.J. Morrissey, A.M. Amthor et al., Evidence for a change in the nuclear mass surface with the discovery of the most neutron-rich nuclei with $17 \leq Z \leq 25$. *Phys. Rev. Lett.* **102**, 142501 (2009). doi:[10.1103/PhysRevLett.102.142501](https://doi.org/10.1103/PhysRevLett.102.142501)
18. J.M. D’Auria, A review of radioactive beam facilities in the world. *Nucl. Instrum. Methods B* **99**, 330 (1995). doi:[10.1016/0168-583X\(95\)80083-2](https://doi.org/10.1016/0168-583X(95)80083-2)
19. T. Motobayashi, H. Sakurai, Research with fast radioactive isotope beams at RIKEN. *Prog. Theor. Exp. Phys.* **2012**, 03C001 (2012). doi:[10.1093/ptep/pts059](https://doi.org/10.1093/ptep/pts059)
20. W. Loveland, Synthesis of transactinide nuclei using radioactive beams. *Phys. Rev. C* **76**, 014612 (2007). doi:[10.1103/PhysRevC.76.014612](https://doi.org/10.1103/PhysRevC.76.014612)
21. M.H. Mun, G.G. Adamian, N.V. Antonenko et al., Toward neutron-rich nuclei via transfer reactions with stable and radioactive beams. *Phys. Rev. C* **91**, 054610 (2015). doi:[10.1103/PhysRevC.91.054610](https://doi.org/10.1103/PhysRevC.91.054610)
22. J.C. Yang, J.W. Xia, G.Q. Xiao et al., High intensity heavy ion accelerator facility (HIAF) in China. *Nucl. Instrum. Methods B* **317**, 263 (2013). doi:[10.1016/j.nimb.2013.08.046](https://doi.org/10.1016/j.nimb.2013.08.046)
23. L.J. Mao, J.C. Yang, J.W. Xia et al., Electron cooling system in the booster synchrotron of the HIAF project. *Nucl. Instrum. Methods A* **786**, 91 (2015). doi:[10.1016/j.nima.2015.03.052](https://doi.org/10.1016/j.nima.2015.03.052)
24. N. Wang, E.G. Zhao, W. Scheid et al., Theoretical study of the synthesis of superheavy nuclei with $Z = 119$ and 120 in heavy-ion reactions with trans-uranium targets. *Phys. Rev. C* **85**, 041601(R) (2012). doi:[10.1103/PhysRevC.85.041601](https://doi.org/10.1103/PhysRevC.85.041601)
25. Z.Q. Feng, G.M. Jin, F. Fu et al., Production cross sections of superheavy nuclei based on dinuclear system model. *Nucl. Phys. A* **771**, 50 (2006). doi:[10.1016/j.nuclphysa.2006.03.002](https://doi.org/10.1016/j.nuclphysa.2006.03.002)
26. X.J. Bao, Y. Gao, J.Q. Li et al., Possibilities for synthesis of new isotopes of superheavy nuclei in cold fusion reactions. *Phys. Rev. C* **93**, 044615 (2016). doi:[10.1103/PhysRevC.93.044615](https://doi.org/10.1103/PhysRevC.93.044615)
27. Z.Q. Feng, G.M. Jin, J.Q. Li, Production of heavy isotopes in transfer reactions by collisions of $^{238}\text{U} + ^{238}\text{U}$. *Phys. Rev. C* **80**, 067601 (2009). doi:[10.1103/PhysRevC.80.067601](https://doi.org/10.1103/PhysRevC.80.067601)
28. M.H. Mun, G.G. Adamian, N.V. Antonenko et al., Production cross section of neutron-rich isotopes with radioactive and stable beams. *Phys. Rev. C* **89**, 034622 (2014). doi:[10.1103/PhysRevC.89.034622](https://doi.org/10.1103/PhysRevC.89.034622)
29. L. Zhu, Z.Q. Feng, F.S. Zhang, Production of heavy neutron-rich nuclei in transfer reactions within the dinuclear system model. *J. Phys. G* **42**, 085102 (2015). doi:[10.1088/0954-3899/42/8/085102](https://doi.org/10.1088/0954-3899/42/8/085102)
30. S. Ayik, B. Schürmann, W. Nörenberg, Microscopic transport theory of heavy-ion collisions I. Basic relations and transport coefficients for symmetric fragmentation. *Z. Phys. A* **277**, 299 (1976). doi:[10.1007/BF01415605](https://doi.org/10.1007/BF01415605)
31. Z.Q. Feng, G.M. Jin, J.Q. Li et al., Formation of superheavy nuclei in cold fusion reactions. *Phys. Rev. C* **76**, 044606 (2007). doi:[10.1103/PhysRevC.76.044606](https://doi.org/10.1103/PhysRevC.76.044606)
32. G.G. Adamian, N.V. Antonenko, W. Scheid, Characteristics of quasifission products within the dinuclear system model. *Phys. Rev. C* **68**, 034601 (2003). doi:[10.1103/PhysRevC.68.034601](https://doi.org/10.1103/PhysRevC.68.034601)
33. Z.Q. Feng, Production of neutron-rich isotopes around $N = 126$ in multinucleon transfer reactions. *Phys. Rev. C* **95**, 024615 (2017). doi:[10.1103/PhysRevC.95.024615](https://doi.org/10.1103/PhysRevC.95.024615)
34. G.G. Adamian, N.V. Antonenko, V.V. Sargsyan et al., Possibility of production of neutron-rich Zn and Ge isotopes in multinucleon transfer reactions at low energies. *Phys. Rev. C* **81**, 024604 (2010). doi:[10.1103/PhysRevC.81.024604](https://doi.org/10.1103/PhysRevC.81.024604)
35. R.J. Charity, M.A. McMahan, G.J. Wozniak et al., Systematics of complex fragment emission in niobium-induced reactions. *Nucl. Phys. A* **483**, 371 (1988). doi:[10.1016/0375-9474\(88\)90542-8](https://doi.org/10.1016/0375-9474(88)90542-8)
36. W. Królas, R. Broda, B. Fornal et al., Dynamical deformation of nuclei in deep-inelastic collisions: a gamma coincidence study of $^{130}\text{Te} + 275\text{ MeV } ^{64}\text{Ni}$ and $^{208}\text{Pb} + 345\text{ MeV } ^{58}\text{Ni}$ heavy ion reactions. *Nucl. Phys. A* **832**, 170 (2010). doi:[10.1016/j.nuclphysa.2009.10.159](https://doi.org/10.1016/j.nuclphysa.2009.10.159)